

Bound-state Effects on Top Quark Production at Hadron Colliders

Kaoru Hagiwara*

KEK Theory Division and Sokendai, Tsukuba 305-0801, JAPAN

Yukinari Sumino†

Dept. of Physics, Tohoku University, Sendai 980-8578, JAPAN

Hiroshi Yokoya‡

Theory Unit, Physics Department, CERN, CH-1211 Geneva, SWITZERLAND

Abstract

We study bound-state effects on the $t\bar{t}$ production cross section in the threshold region at hadron colliders. The bound-state effects are important particularly at the LHC where the gluon fusion is the dominant subprocess. Due to the formation of $t\bar{t}$ resonances in the $J = 0$ color-singlet channel of $gg \rightarrow t\bar{t}$ and the large width of the top quark, the $t\bar{t}$ invariant-mass distribution peaks at a few GeV below the $t\bar{t}$ threshold, and it is significantly enhanced over the naive NLO prediction until several GeV above the threshold. We present predictions of the $t\bar{t}$ invariant-mass distribution which incorporate both the bound-state effects and initial-state radiations up to NLO. The bound-state effects would lead to a substantial deformation of top-quark kinematical distributions in the threshold region.

*E-mail address: kaoru.hagiwara@kek.jp

†E-mail address: sumino@tuhep.phys.tohoku.ac.jp

‡E-mail address: hiroshi.yokoya@cern.ch

In the forthcoming CERN Large Hadron Collider (LHC) experiment, top quarks will be produced copiously. A huge top-quark pair production event sample is considered as a good template for performing various physics studies as well as detector calibrations. For this purpose, it is important that we understand physics of the top-quark production and decay accurately. Through dedicated studies of the top-quark pair production events at the Fermilab Tevatron, it has been recognized that top-quark events can be reconstructed with good accuracy. For instance, using a top-quark sample in lepton+4-jet mode, the lepton helicity-angle distribution in top-quark decays has been measured, which requires a full kinematical reconstruction of each event. Up to now, a good agreement with the Standard-Model prediction has been observed for this distribution [1].

At the LHC, top quarks are produced dominantly via gluon-gluon fusion. The gluon distribution function is a rapidly decreasing function of its momentum fraction x . Thus, a substantial amount of top quarks are expected to be pair-produced close to their production threshold in gluon-gluon fusion at the LHC. Therefore, contributions of $t\bar{t}$ resonances may be important in the threshold region. The dominant contribution stems from the $J^{PC} = 0^{-+}$ ($L = S = 0$) color-singlet $t\bar{t}$ resonance states. An effective operator for producing one of these resonances may be written as

$$\mathcal{L}_{gg \rightarrow \phi(t\bar{t})} \propto \epsilon^{\mu\nu\rho\sigma} G_{\mu\nu}^a G_{\rho\sigma}^a \phi(t\bar{t}). \quad (1)$$

In contrast, at the Tevatron, the quark-antiquark fusion is the main process of top production. Hence, the $t\bar{t}$ pairs are predominantly in the color-octet $J = 1$ state, and we anticipate that resonance effects are not significant.

The method for incorporating $t\bar{t}$ bound-state effects has been developed mainly in the studies of $t\bar{t}$ productions in e^+e^- collisions [2, 3]. Formally, in the limit where we neglect the top-quark width, $\Gamma_t \rightarrow 0$, bound-state effects can be incorporated by resummation of the threshold singularities $(\alpha_s/\beta)^n$, where β is the velocity of the top quark in the $t\bar{t}$ c.m. frame. It is known that, due to the large top-quark width, resonance peaks in the top-quark pair production cross section are smeared out, and a broad enhancement of the cross section over the entire threshold region results from the bound-state effects.

On the other hand, a distinct feature of $t\bar{t}$ productions in hadron collisions is that effects of initial-state radiation (ISR) of gluons are significant, especially close to the top pair production threshold [4, 5, 6]. They can be incorporated by resummation of soft and collinear logarithms, which are given in the form $(\alpha_s \ln^2 \beta)^n$. So far, up to our knowledge, only two papers [9, 10] studied bound-state effects on $t\bar{t}$ productions at hadron colliders that are relevant for a realistic top-quark mass.* In Ref. [9], the $t\bar{t}$ invariant-mass distributions are computed in the threshold region incorporating the leading-order (LO) bound-state effects (Coulomb effects) and ignoring other QCD corrections. In Ref. [10], in the study of the total production cross sections of top quarks, the Coulomb effects above

* Earlier works [7, 8] considered production of sharp toponium resonances. Their phenomenology is rather different from that of today's realistic $t\bar{t}$ resonances, which have much larger decay widths.

the $t\bar{t}$ threshold are examined in LO, in comparison to the next-to-leading order (NLO) ISR effects.

In this paper, we study the $t\bar{t}$ invariant-mass distributions in the threshold region, incorporating both bound-state effects and ISR effects at NLO. The differences of the present work from the previous ones are as follows. As compared to Ref. [9], we incorporate the ISR effects and the NLO corrections to the bound-state effects. As compared to Ref. [10], we examine the $t\bar{t}$ invariant-mass distributions; we include contributions from the resonances below the $t\bar{t}$ threshold; we include the NLO corrections to the bound-state effects.

In the computation of the parton-level cross sections, the bound-state effects and the ISR effects factorize in the LO of the threshold singularities and in the leading-logarithmic (LL) approximation of the soft+collinear singularities [11, 6]:

$$\hat{\sigma}_{\text{ISR}}(\hat{s}; i \rightarrow f) = K_i^{(c)} \int_0^1 dz \hat{\sigma}(s' = z\hat{s}; i \rightarrow f) F_i^{(c)}(z). \quad (2)$$

Here, $\hat{\sigma}(s'; i \rightarrow f)$ is the cross section without ISR ($i = q\bar{q}$ or gg , $f = t\bar{t}$ in various color and J states); $\hat{\sigma}_{\text{ISR}}(\hat{s}; i \rightarrow f)$ is the cross section including the ISR effects. The ISR function $F_i^{(c)}$ depends on the initial-state partons (i) and the color of the final-state $t\bar{t}$ system ($c = 1$ and 8 for color-singlet and octet $t\bar{t}$ states, respectively). $K_i^{(c)}$ denotes the hard-vertex correction factor, which is normalized as $K_i^{(c)} = 1$ in the leading order.

In this paper, for simplicity of our analysis, we include the ISR effects up to NLO. It is known that the differences between the NLO and next-to-leading log (NLL) corrections to the $t\bar{t}$ production cross sections are small, if we ignore bound-state effects [10, 6]. Hence, the NLO approximation may be justified for our first analysis of the threshold cross sections. The ISR functions for the production of various color states up to NLO are given by [8, 12]

$$F_i^{(c)}(z) = \delta(1-z) + \frac{\alpha_s(\mu_F)}{\pi} \left[f_i^{(c)} \left(z, \frac{\mu_F}{2m_t} \right) + k_i^{(c)} \left(\frac{\mu_F}{2m_t} \right) \delta(1-z) \right]. \quad (3)$$

The $\mathcal{O}(\alpha_s)$ terms read[†]

$$f_{gg}^{(1)}\left(z, \frac{\mu_F}{2m_t}\right) = 4C_A \left[\left(\frac{\ln(1-z)}{1-z} \right)_+ - \left(\frac{1}{1-z} \right)_+ \ln\left(\frac{\mu_F}{2m_t}\right) \right], \quad (4a)$$

$$f_{gg}^{(8)}\left(z, \frac{\mu_F}{2m_t}\right) = 4C_A \left[\left(\frac{\ln(1-z)}{1-z} \right)_+ - \left(\frac{1}{1-z} \right)_+ \ln\left(\frac{\mu_F}{2m_t}\right) \right] - C_A \left(\frac{1}{1-z} \right)_+, \quad (4b)$$

$$f_{q\bar{q}}^{(8)}\left(z, \frac{\mu_F}{2m_t}\right) = 4C_F \left[\left(\frac{\ln(1-z)}{1-z} \right)_+ - \left(\frac{1}{1-z} \right)_+ \ln\left(\frac{\mu_F}{2m_t}\right) \right] - C_A \left(\frac{1}{1-z} \right)_+, \quad (4c)$$

$$k_{gg}^{(c)}\left(\frac{\mu_F}{2m_t}\right) = -\beta_0 \ln\left(\frac{\mu_F}{2m_t}\right), \quad (5a)$$

$$k_{q\bar{q}}^{(c)}\left(\frac{\mu_F}{2m_t}\right) = -3C_F \ln\left(\frac{\mu_F}{2m_t}\right), \quad (5b)$$

with $\beta_0 = \frac{11}{3}C_A - \frac{2}{3}n_q$. Here, m_t and μ_F denote the top-quark pole mass and the factorization scale, respectively (we take $\mu_F = m_t$); α_s is the strong coupling constant in the $\overline{\text{MS}}$ scheme; $C_F = 4/3$ and $C_A = 3$ are color factors, and we take the number of light quark flavors to be $n_q = 5$. The plus-distribution is defined in the standard manner.

Let us turn to the threshold cross sections without ISR, $\hat{\sigma}(s'; i \rightarrow f)$. As is well known, the S -wave part of the cross sections are most important in the threshold region. Contributions of $L > 0$ are suppressed at least by $\beta^2 \sim \alpha_s^2$ with respect to the leading S -wave contribution. For individual cross sections, leading S -wave contributions reside in the following channels:

$$i = gg, \quad f = t\bar{t}(L = 0, S = 0, J = 0, \text{ color singlet}); \quad (6a)$$

$$i = gg, \quad f = t\bar{t}(L = 0, S = 0, J = 0, \text{ color octet}); \quad (6b)$$

$$i = q\bar{q}, \quad f = t\bar{t}(L = 0, S = 1, J = 1, \text{ color octet}). \quad (6c)$$

There is no color-singlet channel for $i = q\bar{q}$ at LO. The process $gg \rightarrow t\bar{t}(L = 0, S = J = 1)$ in the color-singlet channel is forbidden due to the angular momentum conservation and Bose statistics (Yang's theorem), and the same applies to the symmetric (d^{abc}) part of the color-octet channel. It is also forbidden in the anti-symmetric (f^{abc}) part of the color-octet channel at LO; this is because it is a naïve- T odd transition and is hence forbidden at LO due to the time-reversal invariance of QCD. We ignore qg subprocess contributions, which are suppressed by $\alpha_s\beta^2$ as compared to the LO contribution.

[†] The leading (double-log) terms $\propto [\ln(1-z)/(1-z)]_+$ of $f_{gg}^{(c)}$ and $f_{q\bar{q}}^{(8)}$ are common to those of the pseudo-scalar Higgs boson production via gluon fusion process [13] and the Drell-Yan process [14], respectively.

Following the standard framework developed for threshold cross sections [2, 3], the S -wave cross section for $i \rightarrow f$ including bound-state effects is given by

$$\hat{\sigma}(s'; i \rightarrow f) = [\hat{\sigma}(s'; i \rightarrow f)]_{\text{tree}} \times \frac{\text{Im}[G^{(c)}(\vec{0}; E)]}{\text{Im}[G_0(\vec{0}; E)]}. \quad (7)$$

The non-relativistic Green functions are defined by

$$\left[(E + i\Gamma_t) - \left\{ -\frac{\nabla^2}{m_t} + V_{\text{QCD}}^{(c)}(r) \right\} \right] G^{(c)}(\vec{x}; E) = \delta^3(\vec{x}), \quad (8)$$

where $E = \sqrt{s'} - 2m_t$ is the c.m. energy of the $t\bar{t}$ system measured from the threshold; $r = |\vec{x}|$; Γ_t is the decay width of the top quark; $V_{\text{QCD}}^{(c)}(r)$ is the QCD potential between the color-singlet ($c = 1$) or color-octet ($c = 8$) static quark-antiquark pair. On the other hand, $G_0(\vec{x}; E)$ is the non-relativistic Green function of a free $t\bar{t}$ pair, which is defined via Eq. (8) after setting $V_{\text{QCD}}^{(c)}(r)$ and Γ_t to zero.

We use the NLO QCD potential, which reads [15]:

$$V_{\text{QCD}}^{(c)}(r; \mu_B) = C^{(c)} \frac{\alpha_s(\mu_B)}{r} \left[1 + \frac{\alpha_s(\mu_B)}{4\pi} \left\{ 2\beta_0 [\ln(\mu_B r) + \gamma_E] + a_1^{(c)} \right\} \right] \quad (9)$$

with

$$C^{(1)} = -C_F, \quad C^{(8)} = \frac{C_A}{2} - C_F, \quad (10)$$

$$a_1^{(1)} = a_1^{(8)} = \frac{31}{9}C_A - \frac{10}{9}n_q, \quad (11)$$

for the $\overline{\text{MS}}$ coupling. Here, $\gamma_E = 0.5772\dots$ denotes the Euler constant. The QCD potential is renormalization-group invariant, and we evaluate the above expression at the Bohr scale of $\mu_B = 20$ GeV, and with $n_q = 5$.

Eq. (7) incorporates the QCD bound-state effects between $t\bar{t}$ up to NLO. It also incorporates the top-quark decay-width effects on the cross section $\hat{\sigma}(s'; i \rightarrow f)$ up to NLO, provided that the $\mathcal{O}(\alpha_s)$ correction to the top-quark decay width is included in Γ_t [2, 16].

We correct the $gg \rightarrow t\bar{t}$ tree-level cross sections in the $J = 0$ color-singlet and octet channels using Eq. (7), since they include all the leading S -wave contributions; we do not include bound-state effects in the $J > 0$ channels. In the $q\bar{q} \rightarrow t\bar{t}$ tree-level cross section, there is only color-octet $J = 1$ channel which contains the S -wave contribution, and hence we correct it by using the octet Green function via Eq. (7).

The S -wave Born cross sections behave as $\hat{\sigma} \propto \alpha_s^2 \beta$ near the threshold ($\beta \ll 1$). Expanding $\hat{\sigma}_{\text{ISR}}$ [Eq. (2)] in α_s , we correctly reproduce the dominant $\mathcal{O}(\alpha_s^3)$ corrections of the NLO cross sections [4], namely, $\alpha_s^3 \beta \ln^2 \beta$, $\alpha_s^3 \beta \ln \beta$ and $\alpha_s^3 \beta^0$ terms. Furthermore, by introducing the following hard-vertex correction factors in Eq. (2), we match $\hat{\sigma}_{\text{ISR}}$ to the NLO cross sections up to the $\alpha_s^3 \beta$ term:

$$K_i^{(c)} = 1 + \frac{\alpha_s(\mu_R)}{\pi} h_i^{(c)} \left(\frac{\mu_R}{m_t} \right) \quad (12)$$

with

$$h_{gg}^{(1)}\left(\frac{\mu_R}{m_t}\right) = C_A \left(1 + \frac{\pi^2}{12}\right) + C_F \left(-5 + \frac{\pi^2}{4}\right) + \beta_0 \ln\left(\frac{\mu_R}{2m_t}\right), \quad (13a)$$

$$h_{gg}^{(8)}\left(\frac{\mu_R}{m_t}\right) = C_A \left(3 - \frac{\pi^2}{24}\right) + C_F \left(-5 + \frac{\pi^2}{4}\right) + \beta_0 \ln\left(\frac{\mu_R}{2m_t}\right), \quad (13b)$$

$$h_{q\bar{q}}^{(8)}\left(\frac{\mu_R}{m_t}\right) = C_A \left(\frac{59}{9} - \frac{\pi^2}{4} + \frac{2\ln 2}{3}\right) + C_F \left(-8 + \frac{\pi^2}{3}\right) - \frac{5}{9}n_q - \frac{8}{9} + \beta_0 \ln\left(\frac{\mu_R}{2m_t}\right). \quad (13c)$$

Here, μ_R denotes the renormalization scale in the $\overline{\text{MS}}$ scheme. (We take $\mu_R = m_t$.) The logarithmic part of $h_i^{(c)}$ in Eqs. (13) are independent of the color of the $t\bar{t}$ system. They cancel the renormalization-scale dependence of the Born cross sections which are proportional to $\alpha_s^2(\mu_R)$. The non-logarithmic part of $h_i^{(c)}$ are extracted from the NLO cross sections for the heavy quarkonium productions; $h_{gg}^{(1)}(1)$ from the results of Refs. [8, 12]; $h_{gg}^{(8)}(1)$ and $h_{q\bar{q}}^{(8)}(1)$ from the results of Ref. [12]. Numerically they read $h_{gg}^{(1)}(1) \approx -3.22$, $h_{gg}^{(8)}(1) \approx -0.92$, and $h_{q\bar{q}}^{(8)}(1) \approx -1.61$. We note that the term $-8/9$ in $h_{q\bar{q}}^{(8)}$ is missing in Ref. [12].* This is due to the fact that non-decoupling effects from heavy-quark loops are incorrectly omitted throughout the computations in Ref. [12].[†]

We can extract $h_{q\bar{q}}^{(8)}(1)$ numerically also from the NLO $q\bar{q} \rightarrow t\bar{t}$ cross section [4], which reads $h_{q\bar{q}}^{(8)}(1) \approx -1.8$. The agreement is fairly good. Similarly, we can extract a color-weighted sum of $h_{gg}^{(c)}(1)$ from the NLO $gg \rightarrow t\bar{t}$ cross section [4] as $\frac{2}{7}h_{gg}^{(1)}(1) + \frac{5}{7}h_{gg}^{(8)}(1) \approx 0.8$, which is quite different from the corresponding value -1.58 that follows from Eqs. (13). Nevertheless, we confirmed that these two rather different values are marginally consistent with each other if we take into account the claimed numerical accuracy of Ref. [4].[‡] We will discuss this issue further at the end of the paper.

In general, non-logarithmic parts of $k_i^{(c)}$ and $h_i^{(c)}$ both contribute to the $\alpha_s^3\beta$ term of the cross section. How to separate non-logarithmic parts of $k_i^{(c)}$ and $h_i^{(c)}$ is scheme dependent. In this paper, we choose a scheme such that non-logarithmic part of $k_i^{(c)}$ is zero; see Eqs. (5).

* The non-decoupling effect of the top-quark loop in the gluon vacuum polarization in the s -channel diagram contributes $2[\Pi_t(s = 4m_t^2) - \Pi_t(s = 0)] = -8/9$, where Π_t is the top quark contribution to the gluon two-point function. The factor of 2 appears since it is a part of the interference terms.

[†]We thank the authors of Ref. [12] for confirming this error in their results. We also thank M. Czakon and A. Mitov for providing the analytic expression of the $\alpha_s^3\beta$ term of the $q\bar{q} \rightarrow t\bar{t}$ cross section, prior to its publication [17], which was crucial for us to identify the source of the discrepancy between Refs. [4] and [12].

[‡]A precise statement is as follows. The present discrepancy corresponds to a 7% difference in terms of a_0 , which is the only parameter contributing to the $\alpha_s^3\beta$ term in the fitting function in Ref. [4]. We have checked that it is possible to shift the value of a_0 by 7% without altering the fitting function more than 1%, which is the accuracy claimed for the fit, if we adjust the remaining parameters appropriately.

Finally, convoluting with the parton distribution functions (PDFs), we obtain the hadronic cross section

$$\sigma(s; i \rightarrow f) = \int_0^1 d\tau \frac{d\mathcal{L}_i}{d\tau}(\tau) \hat{\sigma}_{\text{ISR}}(\hat{s} = \tau s; i \rightarrow f) \quad (14)$$

$$= K_i^{(c)} \int_0^1 d\tau \frac{d\mathcal{L}_i}{d\tau}(\tau) \int_0^1 dz \hat{\sigma}(z\tau s; i \rightarrow f) F_i^{(c)}(z). \quad (15)$$

The partonic luminosity is defined by

$$\frac{d\mathcal{L}_i}{d\tau}(\tau; \mu_F) = \sum_{\{a,b\}} \int dx_1 \int dx_2 f_a(x_1, \mu_F) f_b(x_2, \mu_F) \delta(\tau - x_1 x_2), \quad (16)$$

where the summation is over $\{a, b\} = \{g, g\}$ for $i = gg$, and $\{a, b\} = \{q, \bar{q}\}, \{\bar{q}, q\}$ with $q = \{u, d, s, c, b\}$ for $i = q\bar{q}$. In numerical calculations, we use the CTEQ6M (NLO, standard $\overline{\text{MS}}$ scheme) PDF parametrization [18] at the factorization scale of $\mu_F = m_t$. We present our results in the form of the $t\bar{t}$ invariant-mass distribution, which is, in principle, a measurable quantity from the final-states at hadron colliders:

$$\frac{d\sigma}{dm_{t\bar{t}}} (s, m_{t\bar{t}}^2; i \rightarrow f) = \frac{2m_{t\bar{t}}}{s} \hat{\sigma}(m_{t\bar{t}}^2; i \rightarrow f) \times K_i^{(c)} \int_{\tau_0}^1 \frac{dz}{z} F_i^{(c)}(z) \frac{d\mathcal{L}_i}{d\tau} \left(\frac{\tau_0}{z} \right). \quad (17)$$

Here, $m_{t\bar{t}}$ denotes the invariant-mass of $t\bar{t}$, and $\tau_0 = m_{t\bar{t}}^2/s$. The ISR function $F_i^{(c)}(z)$ is convoluted with the partonic luminosity but not with $\hat{\sigma}$, which is evaluated at fixed $s' = m_{t\bar{t}}^2$.

Our formulas for $\hat{\sigma}(s'; i \rightarrow f)$ rely on the non-relativistic QCD framework [3] and are valid only in the threshold region. More specifically, our formulas are subject to $\mathcal{O}(\alpha_s^3 \beta^2)$ corrections that grow with E (part of NNLO corrections). As a result, the $t\bar{t}$ invariant-mass distributions described above are valid only in the threshold region $\beta \ll 1$; they approach the NLO results of Ref. [19] in the region $\alpha_s \ll \beta \ll 1$ but deviate from the NLO results at higher invariant-mass $\beta \sim \mathcal{O}(1)$. Hence, our predictions should be smoothly interpolated to the corresponding NLO results in the region $\alpha_s \ll \beta \ll 1$. Numerically smooth interpolations may be performed at $m_{t\bar{t}} - 2m_t \sim 5\text{--}20$ GeV.[§]

Below we examine the $t\bar{t}$ invariant-mass distributions numerically. We compare the invariant-mass distributions which include QCD corrections in four different ways:

[§] In this regard, we note that the ratio of the Green functions in Eq. (7) has the following high energy behavior:

$$\frac{\text{Im } G^{(c)}}{\text{Im } G_0} \rightarrow 1 - \frac{\pi}{2} C^{(c)} \alpha_s(\mu_B) + \mathcal{O}(\alpha_s^2) \quad \text{for } E \gg 2m_t \quad (\beta \rightarrow 1).$$

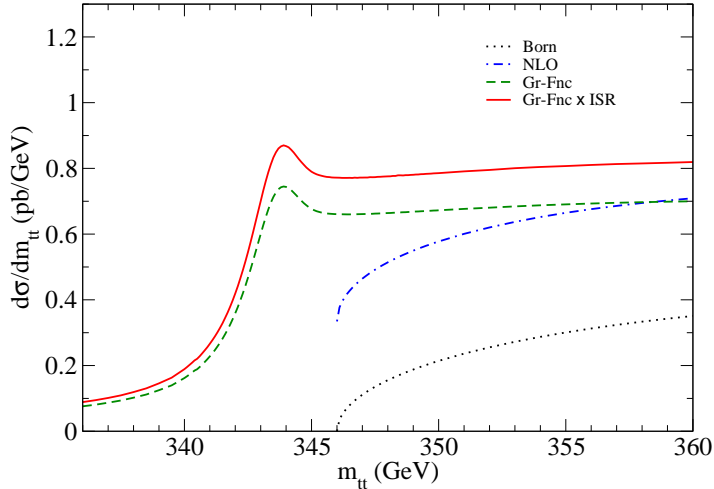


Fig. 1: $t\bar{t}$ invariant-mass distributions for $gg \rightarrow t\bar{t}$ in the threshold region, in the $J = 0$, color-singlet channel at the LHC. The cross sections calculated in the Born approximation (black dotted), with bound-state effects but without ISR effects (green dashed), with ISR effects but without bound-state effects (blue dot-dashed), and with both bound-state and ISR effects (red solid) are plotted. We take $m_t = 173$ GeV and $\Gamma_t = 1.5$ GeV.

- Born: The distribution at the Born level. On the right-hand side of Eq. (17), $\hat{\sigma}$ is replaced by the Born cross section; the ISR function $F_i^{(c)}(z)$ is set to $\delta(1-z)$; the hard-vertex factor $K_i^{(c)}$ is set to 1.
- NLO: The distribution with ISR effects but without bound-state effects. The right-hand side of Eq. (17) (except $d\mathcal{L}_i/d\tau$) is replaced by its expansion in α_s up to $\mathcal{O}(\alpha_s^3)$. Note that it includes the α_s/β part of the Coulomb-gluon exchange effects in $\text{Im}G^{(c)}/\text{Im}G_0$.
- Gr-Fnc: The distribution with bound-state effects but without ISR effects. On the right-hand side of Eq. (17), $F_i^{(c)}(z)$ is set to $\delta(1-z)$ and $K_i^{(c)}$ to 1.
- Gr-Fnc \times ISR: Our full prediction, Eq. (17).

In Fig. 1, we plot the $t\bar{t}$ invariant-mass distributions for $gg \rightarrow t\bar{t}$ in the $J = 0$, color-singlet channel at the LHC. The above four cross sections are shown (dotted, dot-dashed, dashed, and solid lines, respectively), for $m_t = 173$ GeV and $\Gamma_t = 1.5$ GeV. The effects of Γ_t are included only through the Green function in Eq. (8). The cross sections with binding effects exhibit a resonance peak below the threshold, $m_{t\bar{t}} = 2m_t = 346$ GeV. Due to the large width of the top quark, multiple resonance peaks are smeared out and only the broad $1S$ peak remains in $d\sigma/dm_{t\bar{t}}$; the feature well-known in the total cross section for $e^+e^- \rightarrow t\bar{t}$.

The peak position is at $E = m_{t\bar{t}} - 2m_t = -2.1$ GeV, which is very close to

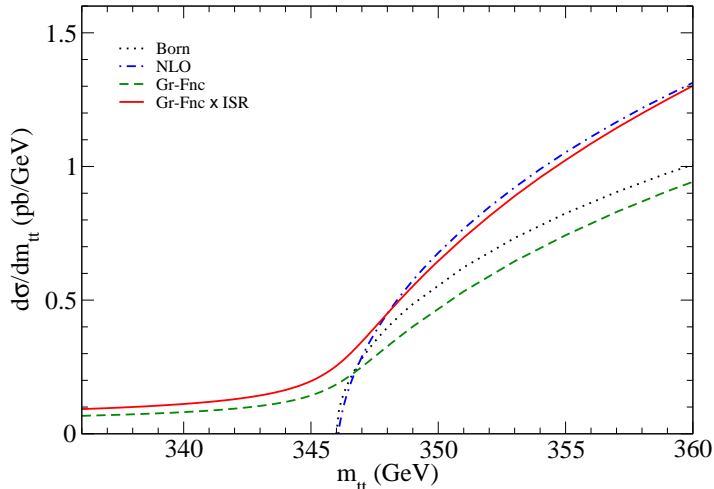


Fig. 2: Same as Fig. 1, but for $gg \rightarrow t\bar{t}$ in the color-octet channel and all J states are summed.

the peak position of the singlet Green function $\text{Im} G^{(1)}$. In fact, the rapid fall off of the partonic luminosity $d\mathcal{L}_i/d\tau$ reduces the peak position by only about a few tens MeV. On the other hand, the ISR effects scarcely change the peak position. This means that the peak positions of the $t\bar{t}$ invariant-mass distributions in the color-singlet channels are, to a very good approximation, the same in e^+e^- and hadron collider experiments.

The ISR effects enhance the invariant-mass distribution obtained with only the bound-state effects (Gr-Fnc) almost independently of $m_{t\bar{t}}$, where the enhancement factor is about 1.2. We also observe that the enhancement by ISR effects is much more pronounced without the bound-state effects than after inclusion of bound-state effects. Namely, the ratio of the approximations NLO and Born is much larger than that of Gr-Fnc \times ISR and Gr-Fnc. This is because a substantial part of the former enhancement comes from the α_s/β term included in NLO, which is genuinely a part of bound-state effects, whereas this term is included in the Gr-Fnc approximation.

Fig. 2 shows the invariant-mass distribution in the gg channel as in Fig. 1, but for the color-octet states and when all J contributions are summed. We have included bound-state effects only in the $J = 0$ channel. By comparing Gr-Fnc \times ISR (solid) and NLO (dot-dashed), one finds that the bound-state effects are not significant. More precisely, among the bound-state effects $(\alpha_s/\beta)^n$, contributions from $n \geq 2$ are rather small for the color-octet state. A small tail of the cross section below the threshold originates from the large width of the top quark. The ratio of Gr-Fnc \times ISR and Gr-Fnc is almost independent of $m_{t\bar{t}}$ and about 1.4.

The striking difference of the bound-state effects in the color-singlet and color-octet channels can be understood as follows. The force between t and \bar{t} is attractive in the color-singlet channel, leading to formation of resonance

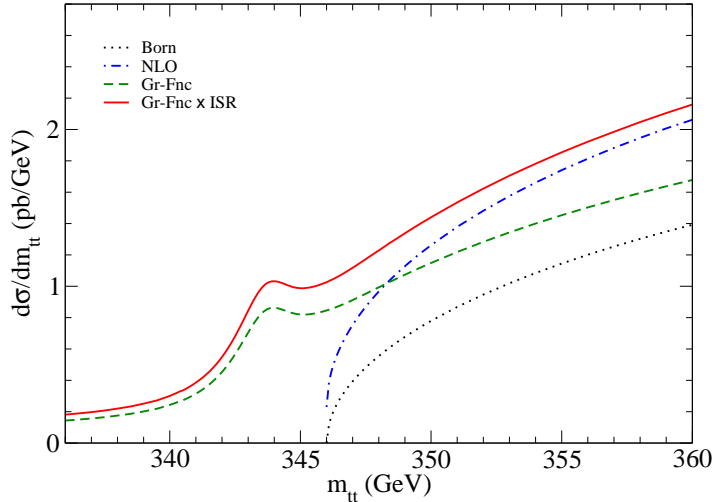


Fig. 3: Same as Fig. 1 ($gg \rightarrow t\bar{t}$), but the color and J are summed.

states below the threshold $m_{t\bar{t}} < 2m_t$. On the other hand, the interquark force is repulsive in the color–octet channel and affects only the continuum states weakly.

Fig. 3 shows a similar comparison of the $t\bar{t}$ invariant-mass distributions after the sum of the color–singlet and color–octet for all J states are taken, for the gg initial state. They are obtained as the sum of the corresponding distributions in Fig. 1 (color–singlet, $J = 0$), those in Fig. 2 (color–octet, all J), and the small contributions of $J \geq 2$ states in the color–singlet channel, which are not shown separately.

Fig. 4 is for the $q\bar{q}$ initial state, where only the color–octet $J = 1$ channel exists. Each distribution is similar to the corresponding one in the color–octet $gg \rightarrow t\bar{t}$ channel, see Fig. 2. Note, however, that the $q\bar{q}$ channel gets smaller enhancement by ISR than the gg color–octet channel does (the ratio of Gr–Fnc \times ISR and Gr–Fnc is about 1.1 for the $q\bar{q}$ channel, whereas the ratio is about 1.4 for the color–octet gg channel.). The difference of the enhancement factors originates from the different color factors in the ISR functions, see Eqs. (3–5).

Displayed in Fig. 5 are the invariant-mass distributions for $t\bar{t}$ pair production at the LHC, where we show explicitly the individual contributions from the gg color–singlet (dashed), gg color–octet (dot-dashed), and $q\bar{q}$ (dotted) channels, as well as the sum of them (solid). Thick lines include both bound-state and ISR effects (Gr–Fnc \times ISR), while thin lines represent the NLO cross sections. The invariant-mass distribution for the sum of all channels still exhibits the $1S$ peak below the $t\bar{t}$ threshold, while it gradually approaches the NLO distribution above the threshold. The color–singlet ($J=0$) gg channel dominates the cross section below and near the $t\bar{t}$ threshold, while the color–octet gg channel is dominant above the threshold. We expect that the cross section below the threshold[¶] ($336 \text{ GeV} < m_{t\bar{t}} < 2m_t = 346 \text{ GeV}$) is about 6 pb, or 6×10^4 events with 10 fb^{-1} .

[¶] The validity range of our formula is given by $|m_{t\bar{t}} - 2m_t| \lesssim \alpha_s^2 m_t$, which is of order 5–10 GeV.

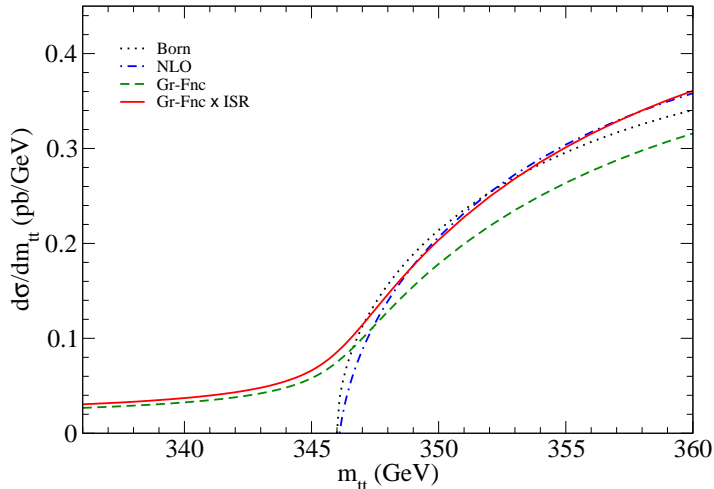


Fig. 4: Same as Fig. 3, but in $q\bar{q}$ channel (color-octet and $J = 1$).

The total enhancement due to the binding effects ($-10 \text{ GeV} < m_{t\bar{t}} - 2m_t < 10 \text{ GeV}$) is estimated to be about 8 pb, which corresponds to 1% of the total NLO cross section. It will be important to take them into account in detector-response calibration and in the precise measurements of the top-quark mass.

Fig. 6 is the same as Fig. 5 but for the Tevatron, $p\bar{p}$ collision at $\sqrt{s} = 1.96 \text{ TeV}$. Due to the dominance of $q\bar{q}$ channel which is color-octet in the leading order, bound-state effects are less significant in the threshold region. The increase of the cross section *above* the threshold due to bound-state effects, as defined by the difference between Gr-Fnc \times ISR and NLO cross sections at $0 < m_{t\bar{t}} - 2m_t < 10 \text{ GeV}$, is about 0.01 pb. The ratio to the total cross section in NLO [4] is 2×10^{-3} , which is consistent with the corresponding value of Ref. [10]. However, the $t\bar{t}$ pair-production cross section *below* the threshold ($-10 \text{ GeV} < m_{t\bar{t}} - 2m_t < 0$) is estimated to be about 0.07 pb, or 70 events with 1 fb^{-1} . Even though their contribution is still a small fraction, a few clean events in this region could significantly affect the top-quark mass determination at the Tevatron.

We may summarize the new aspects of our predictions over the previous works as follows. The most important difference of our predictions compared to those of Ref. [9] is the inclusion of ISR effects. These effects increase the invariant-mass distributions (Gr-Fnc) almost independently of $m_{t\bar{t}}$ by about 20%, 40%, and 10% for the $gg \rightarrow t\bar{t}$ color-singlet, color-octet, and $q\bar{q} \rightarrow t\bar{t}$ color-octet channels, respectively. Furthermore, our predictions are more stable against variations of μ_F , μ_B or μ_R , since we include the NLO corrections to bound-state effects and ISR effects, while only LO bound-state effects are incorporated in Ref. [9]. Concerning the estimates of bound-state effects on the $t\bar{t}$ total cross sections in Ref. [10], we find that they are significant underestimates, since only the effects above the threshold have been taken into account.

Summing up, we find that the bound-state effects significantly alter the

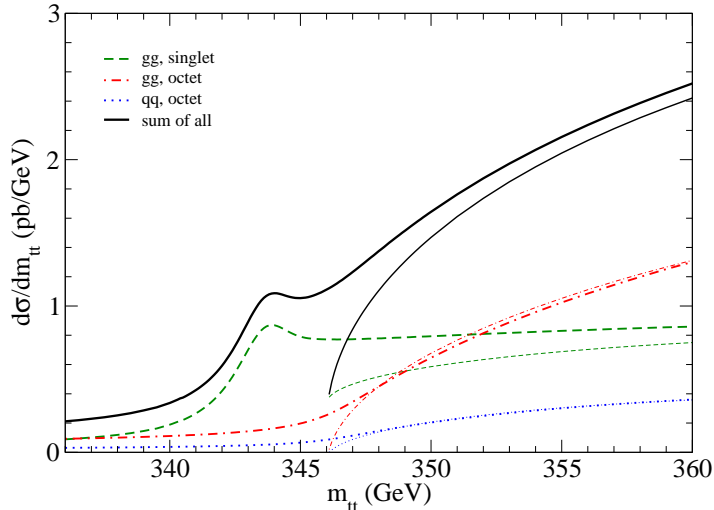


Fig. 5: $t\bar{t}$ invariant-mass distributions for the top-quark production in the threshold region at LHC. The color-singlet (green dashed) and octet (red dot-dashed) in gg channel, color-octet in $q\bar{q}$ channel (blue dotted), and the sum of them (black solid) are plotted. Thick lines include both bound-state and ISR effects, while thin lines represent the cross sections with only NLO effects.

invariant-mass distributions of the $t\bar{t}$ production close to the threshold at the LHC. The effects will be particularly important for the determination of the top-quark mass [19], as well as when the top-quark sample is to be used for calibration of jet energy scale, etc. at an early stage of the LHC operation. In this regard, it should be noted (known from the studies of $e^+e^- \rightarrow t\bar{t}$ [20]) that the bound-state effects distort the momentum distribution of top quarks strongly below the threshold ($m_{t\bar{t}} < 2m_t$). On the other hand, Tevatron experiments are almost free from the bound-state effects, because of the dominance of the color-octet $q\bar{q}$ annihilation contribution, as can be seen from Fig. 6.

We consider that our calculations incorporate the most important part of the bound-state effects and ISR effects to the $t\bar{t}$ threshold cross sections at hadron colliders. There are, however, many corrections that should be included to make the predictions more precise. Among them are resummation of the collinear and soft logarithms (beyond NLO), non-factorizable corrections, etc. They are expected to modify our results at the level of 10–30%. Furthermore, as already stated, presently there remains a considerable disagreement in a color-weighted sum of the hard-vertex factors $h_{gg}^{(c)}$. Hence, we examined the following case separately: we use the value of $h_{gg}^{(1)}$ as in Eq. (13a), which is determined from the two mutually consistent results [8, 12]; on the other hand, we determine the value of $h_{gg}^{(8)}$ such that the $\alpha_s^3\beta$ term of the $gg \rightarrow t\bar{t}$ cross section of Ref. [4] is reproduced, i.e. $h_{gg}^{(8)}(1) \approx 2.39$. With this value of $h_{gg}^{(8)}$, the cross section in the gg color-octet channel is enhanced by about 10% as compared to the case with $h_{gg}^{(8)}(1) \approx -0.92$.

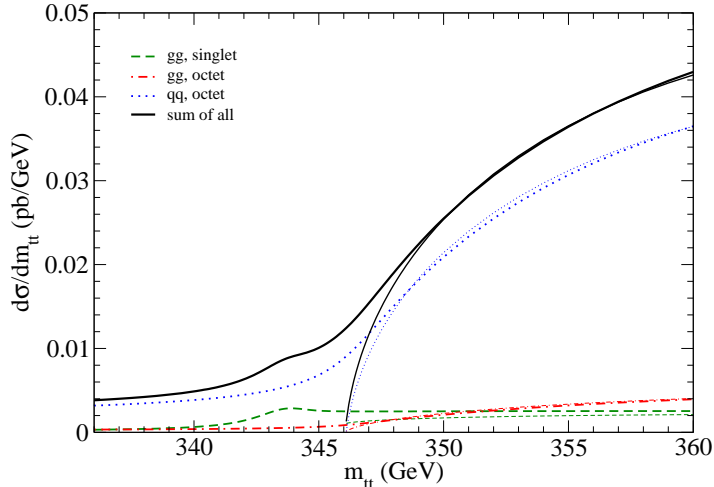


Fig. 6: Same as Fig. 5, but for the cross section at Tevatron.

As a result, the cross section for ‘sum of all’ in Fig. 5 becomes more enhanced as $m_{\bar{t}t}$ increases, where the enhancement is less than 2% below the threshold, and is about 6% at $m_{\bar{t}t} = 360$ GeV. By contrast, the cross section for ‘sum of all’ in Fig. 6 scarcely changes. We also varied $\mu_R = \mu_F$ between $m_t/2$ and $2m_t$ and found that the normalization of the cross sections changes by about 10% accordingly.

We are grateful to the referee for drawing our attention to Ref. [12]. We are also grateful to M. Czakon, A. Mitov and the authors of Refs. [4, 12] (especially M. Mangano, F. Maltoni and P. Nason) for valuable communications. The works of K.H. and Y.S. are supported in part by Grant-in-Aid for scientific research (Nos. 17540281 and 17540228, respectively) from MEXT, Japan. We thank M. Nojiri for organizing an LHC-focus week meeting at the IPMU (Institute for the Physics and Mathematics of the Universe) in December 2007, where we enjoyed stimulating discussions.

References

- [1] A. Abulencia *et al.* [CDF II Collaboration], Phys. Rev. D **75** (2007) 052001 [arXiv:hep-ex/0612011]; V. M. Abazov *et al.* [D0 Collaboration], Phys. Rev. Lett. **100**, 062004 (2008) [arXiv:0711.0032 [hep-ex]].
- [2] V. S. Fadin and V. A. Khoze, JETP Lett. **46** (1987) 525 [Pisma Zh. Eksp. Teor. Fiz. **46** (1987) 417].
- [3] A. H. Hoang *et al.*, Eur. Phys. J. direct C **2** (2000) 1 [arXiv:hep-ph/0001286], and references therein.
- [4] P. Nason, S. Dawson and R. K. Ellis, Nucl. Phys. B **303** (1988) 607.

- [5] W. Beenakker, H. Kuijf, W. L. van Neerven and J. Smith, *Phys. Rev. D* **40** (1989) 54.
- [6] R. Bonciani, S. Catani, M. L. Mangano and P. Nason, *Nucl. Phys. B* **529** (1998) 424 [arXiv:hep-ph/9801375].
- [7] G. Pancheri, J. P. Revol and C. Rubbia, *Phys. Lett. B* **277**, 518 (1992).
- [8] J. H. Kühn and E. Mirkes, *Phys. Rev. D* **48**, 179 (1993) [arXiv:hep-ph/9301204].
- [9] V. S. Fadin, V. A. Khoze and T. Sjostrand, *Z. Phys. C* **48** (1990) 613.
- [10] S. Catani, M. L. Mangano, P. Nason and L. Trentadue, *Phys. Lett. B* **378** (1996) 329 [arXiv:hep-ph/9602208].
- [11] G. T. Bodwin, E. Braaten and G. P. Lepage, *Phys. Rev. D* **51**, 1125 (1995) [Erratum-ibid. *D* **55**, 5853 (1997)] [arXiv:hep-ph/9407339].
- [12] A. Petrelli, M. Cacciari, M. Greco, F. Maltoni and M. L. Mangano, *Nucl. Phys. B* **514** (1998) 245 [arXiv:hep-ph/9707223].
- [13] M. Spira, A. Djouadi, D. Graudenz and P. M. Zerwas, *Phys. Lett. B* **318** (1993) 347.
- [14] G. Altarelli, R. K. Ellis and G. Martinelli, *Nucl. Phys. B* **157** (1979) 461.
- [15] B. A. Kniehl, A. A. Penin, Y. Schroder, V. A. Smirnov and M. Steinhauser, *Phys. Lett. B* **607**, 96 (2005) [arXiv:hep-ph/0412083], and references therein.
- [16] K. Melnikov and O. I. Yakovlev, *Phys. Lett. B* **324**, 217 (1994) [arXiv:hep-ph/9302311]; Y. Sumino, Ph.D. thesis, University of Tokyo, 1993.
- [17] M. Czakon and A. Mitov, in preparation.
- [18] J. Pumplin, D. R. Stump, J. Huston, H. L. Lai, P. Nadolsky and W. K. Tung, *JHEP* **0207** (2002) 012 [arXiv:hep-ph/0201195].
- [19] R. Frederix and F. Maltoni, arXiv:0712.2355 [hep-ph]; See also, J. M. Campbell and R. K. Ellis, *Phys. Rev. D* **60** (1999) 113006.
- [20] Y. Sumino, K. Fujii, K. Hagiwara, H. Murayama and C. K. Ng, *Phys. Rev. D* **47** (1993) 56; M. Jezabek, J. H. Kühn and T. Teubner, *Z. Phys. C* **56**, 653 (1992).